American Mineralogist, Volume 83, pages 762–774, 1998

Characterization of mixed-layer illite-smectite from bentonites using microscopic, chemical, and X-ray methods: Constraints on the smectite-to-illite transformation mechanism

JAVIER CUADROS* and STEPHEN P. ALTANER

Department of Geology, University of Illinois, Urbana, Illinois 61801, U.S.A.

ABSTRACT

We studied mixed-layer illite-smectite (I/S) (<1 or 0.5 μm size fractions) in 28 diagenetic bentonite samples, Pliocene to Ordovician in age, from different locations in North America and Europe to investigate the smectite-to-illite transformation mechanism. XRD-measured illite contents ranged from 3 to 100%, and layer ordering varied continuously from R = 0 to R ≥ 3. XRD polytype analysis showed that with progressive illitization, I/S changes from a predominantly cis-vacant to a trans-vacant structure, although considerable scatter is present in the data. There is no evolution of illite in the I/S from $1M_d$ to $1M$ polytypes with progressive illitization. Microprobe chemical analysis and combustion analysis for N showed that NH_4^+ comprised 9–22% of the total fixed cation content. We calculated an interlayer charge for the illite end-member of 1.5 per $O_{20}(OH_4)$. Sample morphology was studied by atomic force microscopy, which showed a constant aspect ratio and particle diameter over the whole I/S series. Particle thickness increased with percent illite. Oxygen isotope compositions of the I/S clays did not display any systematic trends. Our results suggest that illitization of bentonite I/S proceeds via a solid-state mechanism, with local lattice rearrangements that permit structural (octahedral cis/trans occupancy) and chemical changes in 2:1 layers and cause interlayer coalescence.

INTRODUCTION

The mechanism of the transformation of smectite into illite is key to understanding the thermodynamic relationship among the minerals in the transformation sequence (smectite, I/S of different compositions, and illite) and the detailed kinetics (not only the overall kinetics) of the process. Many studies have shown that two main mechanisms operate during the transformation: solid-state transformation (SST) and; dissolution followed by precipitation (DP). The first mechanism (Shutov et al. 1969; Dunoyer de Segonzac 1970; Hower et al. 1976) involves illitization in the solid state, with the gradual replacement of smectite by illite on a layer-by-layer basis. In this process, which typically also involves fluids that can act as catalysts and transport media, the replacement of smectite by illite occurs in close topotactic contact. The second mechanism involves complete dissolution of smectite followed by precipitation of I/S or illite. This process allows major changes in structure and texture to occur as illitization proceeds so that the structural memory of the precursor mineral is lost. Two main versions of the DP mechanism have been described, including: (1) progressive dissolution of smectite in a reaction front on a very small scale with in situ precipitation of the new phase (Ahn and Peacor 1986); and (2) initial dissolution of smectite followed by progressive coarsening of illite governed by an Ostwald ripening process (Eberl and Środoń 1988; Eberl et al. 1990).

Many authors have reported evidence supporting one or the other reaction mechanism. In many cases the SST mechanism was proposed for materials with low permeability such as bentonite (Altaner et al. 1984; Środoń et al. 1986; Inoue et al. 1990; Elliott et al. 1991), shale and bentonite (Bell 1986), and mudstone (Lindgreen and Hansen 1991; Lindgreen et al. 1991). Support for this mechanism was found by the mentioned authors in older K-Ar ages for more illitic I/S; chemical composition of samples showing preservation of illite layers formed in the earlier steps of the transformation or progressive changes in the I/S composition; I/S interlayer ordering suggesting a gradual transformation; and absence of morphological and crystallographic changes during illitization. Conversely, the DP mechanism has been proposed for environments of higher permeability, such as hydrothermal systems (Inoue 1986; Yau et al. 1987; Inoue et al. 1988; Kitagawa et al. 1994; Inoue and Kitagawa 1994). These authors found support for this mechanism mainly in the morphological changes undergone by the clay particles during illitization and also in the spatial relationships between smectitic and illitic particles in undisturbed clay separates. Robert et al. (1991) proposed that higher tem-

* Present address: Departamento de Ciencias de la Tierra y Química Ambiental, Estación Experimental del Zaidín. Profesor Albareda 1. E-18008 Granada, Spain.
E-mail: jcuadros@eez.csic.es

0003–004X/98/0708–0762$05.00

perature also favors the DP mechanism. Many authors conclude that both mechanisms are possible and that they are controlled by rock permeability (Inoue et al. 1990; Yau et al. 1987; Inoue and Kitagawa 1994), temperature (Robert et al. 1991), or both (Harvey and Browne 1991). Eberl (1993) proposed a transition from SST to DP with depth in the Gulf of Mexico, and related the change in mechanism to acidity generated during organic maturation.

In any case, it is difficult to determine the precise conditions that favor one mechanism over the other. Some authors have found evidence for a DP mechanism in bentonite (Nadeau et al. 1985; Šucha et al. 1993), mudstone (Buatier et al. 1992; Awwiller 1993), and shale (Šucha et al. 1993). Moreover, there are reports of lithologies in which both mechanisms seem to occur, including sandstone and shale studied by Pollastro (1985) and a hydrothermal system studied by Amouric and Olives (1991), as indicated by scanning electron microscopy (SEM) and high resolution transmission electron microscopy (HRTEM), respectively.

It is important to realize that formation of I/S or illite in hydrothermal systems may not necessarily follow a pathway of progressive illitization of smectite. For example, hydrothermal alteration of volcanic rocks may involve I/S formation directly from a glass precursor rather than from a smectite precursor (Lanson and Champion 1991).

There are numerous closed-system experimental studies of smectite illitization that include interpretations about the possible reaction mechanisms for illitization (Eberl 1978; Roberson and Lahann 1981; Whitney 1990, 1992); however, we question the application of those studies to natural systems. The actual extent of illitization is unclear in many of those studies because reaction products, which generally are not analyzed chemically, become expandable when exchanged with cations such as Ca, Mg, or Na (Whitney and Northrop 1988; Huang et al. 1993). This was corroborated by Cuadros and Linares (1996), who characterized the extent of illitization using several analytical techniques and found a maximum transformation of about 0.3% of the original smectite in their hydrothermal experiments.

In this paper, we characterize diagenetically transformed bentonites having a wide range of illite contents by means of numerous mineralogic, microscopic, and geochemical techniques. For an SST mechanism, one expects gradual changes in mineralogy, crystal structure, chemical composition, and oxygen isotopic composition as illitization proceeds, whereas for the DP mechanism, one expects such changes to be abrupt. In addition, large-scale changes in structure and composition support a DP mechanism, whereas small-scale changes (on the order of 1 nm) indicate that an SST mechanism operated. These small-scale changes might be detected by HRTEM, analytical electron microscopy, and electron diffraction. The different analytical techniques used in this work (XRD analysis of polytype, chemical, thermal, morphological, and oxygen isotope analysis) show whether these changes are gradual, abrupt, or even non-existent, thus supporting one or the other transformation mechanism. Our results indicate that smectite transforms into illite through a solid state process in the bentonite samples investigated in this study.

TABLE 1. Sample labels, geologic age, and location of the studied bentonites, as well as references to previous studies

S-2	Pliocene	Almería, Spain*
1-87	Miocene	Oregon, U.S.A.†
2-86	Miocene	Oregon, U.S.A.
9	Cretaceous	Montana, U.S.A.‡
11a	Cretaceous	Montana, U.S.A.
11b	Cretaceous	Montana, U.S.A.
14b	Cretaceous	Montana, U.S.A.
82-2s	Cretaceous	Montana, U.S.A.
82-16-11b	Cretaceous	Montana, U.S.A.
82-17ff	Cretaceous	Montana, U.S.A.
82-19g	Cretaceous	Montana, U.S.A.
83-1e	Cretaceous	Montana, U.S.A.
R-80	Carboniferous	Silesia, Poland§
82-29	Devonian	Virginia, U.S.A.‡
82-32o	Devonian	Virginia, U.S.A.
82-32u	Devonian	Virginia, U.S.A.
82-36a	Devonian	New York, U.S.A.‡
82-36b	Devonian	New York, U.S.A.
82-37c	Devonian	New York, U.S.A.
82-38	Devonian	New York, U.S.A.
NI-6	Silurian	Northern Ireland‖
WDH-25	Silurian	Newton, U.K.‖
3-1	Ordovician	Quebec, Canada#
26-59	Ordovician	Quebec, Canada#
26-171	Ordovician	Quebec, Canada#
CPO-5	Ordovician	Northern Ireland**
SWE-79	Ordovician	Sweden††
WAL-14	Ordovician	Wales‡‡

* Cuadros and Linares 1996.
† Altaner and Grim 1990.
‡ Altaner 1985.
§ Środoń et al. 1986.
‖ Cetin and Huff 1995.
Brun and Chagnon 1979.
** Cameron and Anderson 1980.
†† Bergstrom and Nilsson 1974.
‡‡ Smallwood 1986.

MATERIALS AND METHODS

We studied 28 bentonite samples of various geologic ages from diverse geographic locations (Table 1). Most of the bentonite beds were 5 to 20 cm thick. However, sample S-2 is from a 30 m thick bed; samples 1-87 and 2-86 are from a 15 m thick bed; samples 11a, 11b, 82-2s, and 83-1e are from a 2.5 m thick bed; and sample R-80 is from a 2 m thick bed. I/S has a burial diagenetic origin in all bentonites (see references in Table 1) except S-2, in which the original tuff was first altered by hydrothermal fluids (~80 °C) and later by meteoric waters (Delgado 1994).

All analyses reported in this work were performed at the University of Illinois except the electron microprobe and oxygen isotope analyses, which were performed at the Department of Geology at the University of Chicago and at the Estación Experimental del Zaidín (CSIC) in Granada (Spain), respectively. Thin sections were studied

by optical microscopy. Rock chips were examined by means of SEM using a JEOL JSM-840A, equipped with an energy-dispersive X-ray analyzer (Kevex 7500). Whole-rock samples were ground in isopropyl alcohol using an agate mill micronizer. The resulting powders were analyzed by X-ray diffraction (XRD) using a Siemens D500 with a Cu-tube, and 1° divergence and receiving slits, at 30 kV and 30 mA, with a step size of 0.04° 2θ and a count time of 1 s. The relative abundance of identified minerals was determined by measuring the integrated areas of selected peaks and normalizing them using an intensity factor for each mineral. The intensity factors correspond to peak intensities relative to the strongest reflection of corundum (I/I_c), which were taken from Bayliss (1986), except for the following: phyllosilicates, $I/I_c = 0.21$ for the 4.5 Å reflection; potassium feldspar, $I/I_c = 2.6$ for the 3.25 Å peak; and anatase, $I/I_c = 1.5$ for the 3.52 Å peak.

For clay mineral analysis, the samples were placed in deionized water, then sonified and centrifuged to the desired size fraction, typically <1 or 0.5 μm. Oriented aggregates were prepared by placing several drops of the sample suspension onto a glass slide and letting them dry. The samples were studied by XRD after air drying, solvating with ethylene glycol (24 h in a 60 °C glycol atmosphere), and heating at 450 °C for 1 h. Some of the <1 μm size fractions contained a small amount of kaolinite; for these, the <0.5 μm size fraction was used. The amount of kaolinite in this fraction was smaller. The abundance of kaolinite was determined from the glycol patterns using integrated peak areas of I/S and kaolinite and mineral intensity factors calculated using the program NEWMOD (Robert C. Reynolds, Dartmouth College). The abundance of kaolinite was <1% in all cases. One sample (82-16-11b) contained calcite, which was removed by dispersing the sample in water and adding dilute HCl until a pH of 4 was reached. The dispersion was constantly stirred. Subsequently, the sample was washed repeatedly with deionized water and centrifuged until no Cl^- could be detected with addition of $AgNO_3$. XRD patterns of this treated sample showed no calcite peaks.

The amount of illite layers in the I/S samples and the Reicheweite (R) ordering factor were determined from the glycol XRD patterns using methods described in Moore and Reynolds (1989). To facilitate maximum random orientation of I/S clay particles, samples were freeze-dried before polytype analysis. We used a Labconco Freezone 6 freeze-dryer. After freeze-drying, the smectite-rich samples had the texture of long, thin interwoven fibers. We repeatedly chopped the samples with a blade to reduce fiber size. The samples were side-loaded in the holder without compression and then studied by XRD at 30 kV and 30 mA, with a 0.05° 2θ step size and 90 s count time. The polytypes were determined by comparing experimental patterns with those calculated using the program WILDFIRE (Reynolds 1993). These data showed the presence of minerals other than I/S (such as anatase, quartz, and calcite; see Table 3 in Cuadros and Altaner 1998) in some of the samples. Their relative amounts were quantified as indicated above for the whole-rock samples.

The I/S samples were chemically analyzed using a Cameca SX-50 microprobe equipped with four wavelength dispersive spectrometers. A relatively low beam current (25 nA with an accelerating voltage of 15 kV) and a defocused beam (50 μm diameter spot size) were used to minimize volatilization of alkali cations (Velde 1984). The samples were prepared as pressed pellets in a 3 mm cylindrical die. Three different spot locations were analyzed in each pellet and the results were averaged. If a significant variation occurred in one of the three analyses, two more analyses were performed, the anomalous analysis was discarded, and the other four were averaged. Typically analyses were reproducible to within a margin of 2% of the determined value. Although the pellets did not have a perfectly flat top surface, Ylagan (1996) found no significant differences in chemical composition of another set of clays using electron microprobe analysis of pressed powder pellets and X-ray fluorescence analysis on fused glass disks.

The I/S samples were also analyzed for N using a Leeman Labs CE440 Elemental Analyzer. In this technique, the samples are heated at ~960 °C, and the amounts of evolved CO_2, H_2O, and N_2 are measured by thermal conductivity (Culmo 1969). The standard error for N is 0.6% of the determined value. N was assumed to correspond to NH_4^+ in the clay interlayer. Infrared spectra of the samples showed the presence of the NH_4^+ band at 1430 cm^{-1}, whose area correlated well with measured N_2.

The chemical results were corrected for mineral impurities quantified in the XRD polytype analysis (2% in weight or less; see Table 3 in Cuadros and Altaner 1998). Corrected chemical data were converted into I/S structural formulae assuming a total negative charge of 44. All Fe was considered to be Fe^{+3}. For the S-2 sample, Mg was distributed between the octahedral sheet and the interlayer using the whole sample wet chemical analysis and exchangeable cation analysis by Cuadros and Linares (1996).

Morphological analysis of I/S particles was performed by atomic force microscopy (AFM) in contact mode, using a Topometrix Explorer with a silicon nitride tip and an air scanner having a movement range $x = y = 2.5$ μm and $z = 0.9$ μm. The analyses were performed under ambient humidity conditions. Relative humidity was not measured but it was very likely 30–50%. Approximately 0.5 mg of I/S clay was dispersed in 10 ml of ultra-deionized water. Samples were not pretreated by cation exchange. Suspensions were sonified for 15 min in a water bath. One drop of the suspension was placed on a freshly cleaved mica surface and dried on a hot plate at ~40 °C. We attempted to measure particle dimensions of at least 60 particles for each sample, although it was not possible in a few cases. We performed our measurements on completely separated, flat-topped particles. The dimensions measured were length (the largest particle axis), width

(the axis perpendicular to length within the particle plate), and thickness. Prior to the measurements, the images were smoothed using the AFM equipment software in order to flatten the background completely. The estimated errors are ±2.1 nm for length or width, and ±0.2 nm for thickness.

For oxygen isotope analysis, I/S samples were heated initially at 130 °C under vacuum for at least 12 h to remove externally adsorbed and interlayer H_2O. Following a method similar to that described by Borthwick and Harmon (1982) and modified by Venneman and Smith (1990), O was extracted by reaction with ClF_3 and converted quantitatively to CO_2 over red-hot graphite. Commercial CO_2 was used as a standard, after being compared with the international standards V-SMOW, SLAP, and GISP. The analyses were performed using a Finnigan-Mat 251 mass spectrometer. All samples were analyzed twice, with a standard deviation <0.4‰ in $\delta^{18}O$. The NBS-28 standard was also analyzed with a measurement deviation below 0.2‰ in $\delta^{18}O$ from the accepted value. All $\delta^{18}O$ values are given relative to SMOW.

Results

Optical microscopy, SEM, and XRD of bulk rocks

Binocular microscopy indicates that samples consist mainly of clay minerals with a variety of accessory phases such as biotite, plagioclase feldspar, and alkali feldspar. Optical microscopy of thin sections confirmed the argillaceous nature of the studied bentonite samples. Relict textures of precursor volcanic glass are only seldom preserved (Fig. 1a). Although clay minerals typically exhibit a massive texture, we assume that volcanic glass was the precursor for most of the clay minerals present in the bentonites. In some cases, alteration of biotite or plagioclase phenocrysts contributes to the clay mineral assemblage (Fig. 1b).

SEM examination revealed I/S morphologies of very fine, irregular, curved flakes or mats of coalesced flakes. In general, flakes seem to be anhedral, but it was difficult to determine their exact texture because of particle coalescence. Our observed clay mineral morphologies are typical for I/S minerals from bentonite (e.g., Keller et al. 1986).

XRD analysis of bulk samples indicates that the bentonites consist mainly of I/S clay minerals with lesser amounts of quartz, plagioclase feldspar, alkali feldspar, and calcite (Table 2). Several samples contain other accessory minerals like pyrite, gypsum, dolomite, and anatase (Table 2).

XRD and chemical analysis of <1 μm size fractions

Our I/S samples span a complete range of illite compositions and Reicheweite (R) values for interlayer ordering (Table 3). The compositions at which there is a transition of R values (e.g., from R0 to R1) are similar to those observed in other studies (Bethke et al. 1986; Inoue et al. 1988; Moore and Reynolds 1989). I/S with

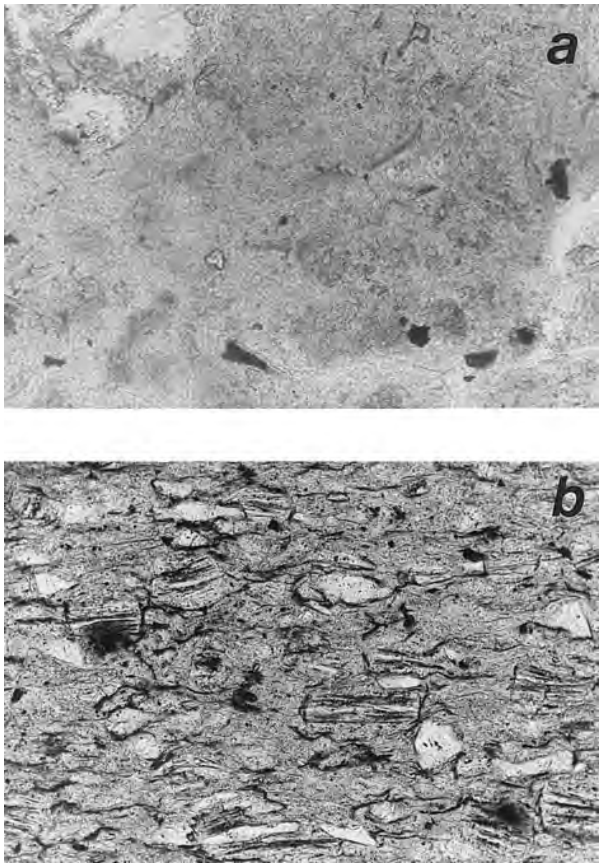

Figure 1. Photomicrographs of bentonite samples in plane polarized light. (**a**) Sample 83-1e (56% I in I/S) shows relict texture of curved glass shards replaced by I/S (light gray). (**b**) Sample 82-36b (87% I) contains abundant biotite altered to I/S.

45% illite (Fig. 2) shows mainly random interlayering, but shows a small development of R1 ordering (e.g., slightly elevated background at 13 and 20 °2θ, the location of the 004 and 006 reflections for rectorite). Samples between 56 and 60% illite (Fig. 2) have R values intermediate between 0 and 1. Samples with 82% and from 86 to 88% illite (Fig. 2) have R values between 1 and 1.5, and 2 to 3, respectively. For 96% illite and above, the I/S ordering cannot be determined using the program NEWMOD.

Polytype analysis was not performed on all I/S samples. Some of them contained other minerals with peaks that interfered with the diagnostic illite polytype peaks (see Table 3 in Cuadros and Altaner 1998). Smectite-rich samples were not analyzed because of turbostratic disorder, which greatly increases error in polytype determination (Reynolds 1993). In simulations done with the program WILDFIRE, the degree of rotational disorder in illite is given by the parameter P_0, which represents the probability of a zero degree rotation between successive 2:1 layers (Reynolds 1993). For $P_0 = 1$, there are no rotations other than zero degrees in the layer stacking sequence, which represents the 1*M* polytype. For $P_0 =$

TABLE 2. Weight percent abundance of minerals in bulk rocks

Sample	I/S	Qtz	Plg	K-sp	Cal	Cri	Py	Gy	Do	Ana
S-2	96	2	1			1				
1-87	98	2								
2-86	95	3	2							
9	95	3	1		1					
11a	90	8	2		tr					
11b	59	39	2		1					
14b	72	3	23			2				
82-2s	72	25	2		1					
82-16-11b	74	2	21		3					
82-17ff	86	3	10					1		
82-19g	73	2	23		2					
83-1e	69	27	3		1					
R-80	91	8		1						
82-29	68	26								6
82-32o	52	48								
82-32u	90	10								
82-36a	93	5	1		1					
82-36b	90	7	2		1					
82-37c	91	3		4				2		
82-38	95	4		2						
NI-6	74	8	17		1					
WDH-25	89	10	1							
3-1	82	17	1							
26-59	70	5	2		16		7			
26-171	81	6	7		4		2			
CPO-5	89	6	1	2					3	
SWE-79	93	5		2						
WAL-14	81	16	3							

Note: I/S = illite-smectite, Qtz = quartz, K-sp = K feldspar, Cal = calcite, Plg = plagioclase, Cri = cristobalite, Py = pyrite, Gy = gypsum, Do = dolomite, Ana = anatase, tr = trace amount.

TABLE 3. Percent illite in I/S, degree of interlayer ordering (R), percent cis-vacancy (vs. trans-vacancy), rotational disorder (P_0), and fraction of 60° rotations (P_{60})

Sample	I (%)	R	Cis (%)	P_0	P_{60}
1-87	3	0			
2-86	10	0			
S-2	16	0			
82-19g*	30	0			
R-80	45	0+	70	0.8	1
83-1e	56	0–1	50	0.75	0.65
82-2s*	57	0–1	55	0.9	0.5
11b*	60	0–1	52	1	0
82-16-11b	62	1			
14b*	64	1			
82-17ff*	65	1			
11a*	68	1	70	0.75	0.3
26-171*	71	1			
3–1*	72	1	70	0.8	0
9*	76	1	60	0.7	0.25
26-59	82	1–1.5	60	0.4	0.5
SWE-79	86	2–3	30	0.75	0.5
82-36b	87	2–3	70	0.6	0
82-38	87	2–3	70	0.57	0.25
82-36a	88	2–3	85	0.52	0.2
82-37c	90	3	85	0.57	0
WDH-25	93	3	30	0.7	0.2
WAL-14*	93	3	40	0.8	0.25
82-32u	93	3	35	0.33	0.3
CPO-5*	96	3 or >3	30	0.75	0.15
NI-6*	97	3 or >3	30	0.8	0.2
82-29	97	3 or >3	45	0.55	0.2
82-32o	100	3 or >3	0		

Note: Asterisk indicates samples with trace amount of kaolinite.

0.33, the rotational disorder is maximum, which corresponds to the $1M_d$ polytype. The rotational disorder is further described with the WILDFIRE parameter P_{60}, which defines the nature of the non-zero degree rotations. For $P_{60} = 1$, all non-zero degree rotations in the stacking sequence are of the n·60° type (n = 1, 2, or 3). For $P_{60} = 0$, all rotations are of the m·120° type (m = 1 or 2).

Figure 3 shows three representative polytype patterns and their corresponding computer simulations. I/S with up to 97% illite has rotational order intermediate between the $1M_d$ (fully disordered) and $1M$ (fully ordered) polytypes (Table 3). There is no systematic relationship between P_0 and percent illite in I/S. In general, the most illitic I/S samples have lower P_{60} values than smectitic I/S. The sample with 100% illite contains a mixture of $1M$ and $2M_1$ illite.

Polytype analysis also gives information about the octahedral sheet structure in terms of cis/trans occupancy. All of our I/S samples are dioctahedral. The octahedral vacancy can be in either the cis-position with respect to the hydroxyls (M2 site) or the trans-position (M1 site, on the mirror plane of the unit cell) (Güven 1988). Roughly, our I/S samples become more trans-vacant with increasing illite (Table 3, Fig. 4). The most illitic sample is a mixture of trans-vacant $1M$ and trans-vacant $2M_1$ illite.

Chemical analysis (Table 4) showed that the I/S samples consist mainly of SiO_2, Al_2O_3, MgO, and Fe_2O_3, with lesser amounts of TiO_2, Na_2O, and CaO. The samples were also analyzed for P, Cl, and S to detect possible contamination. The bold value indicates a suspected con-

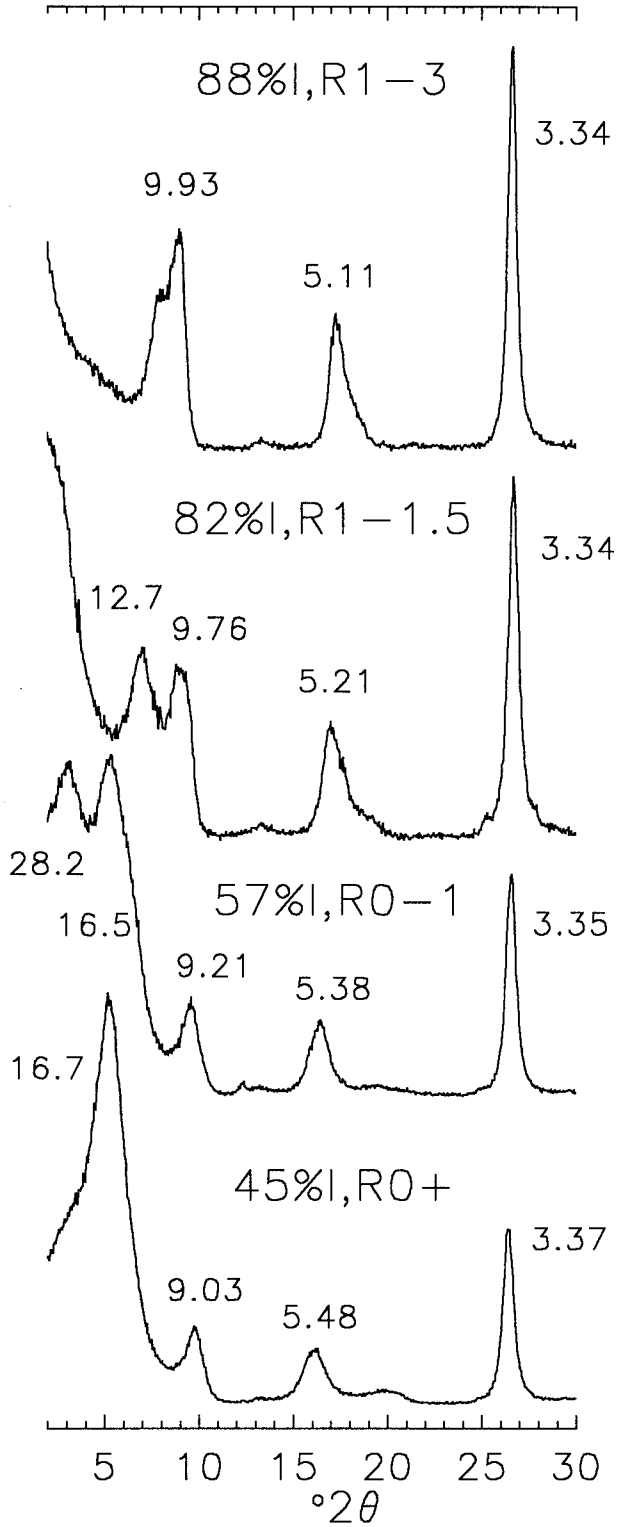

FIGURE 2. XRD patterns of oriented aggregates of glycolated I/S with intermediate ordering (R).

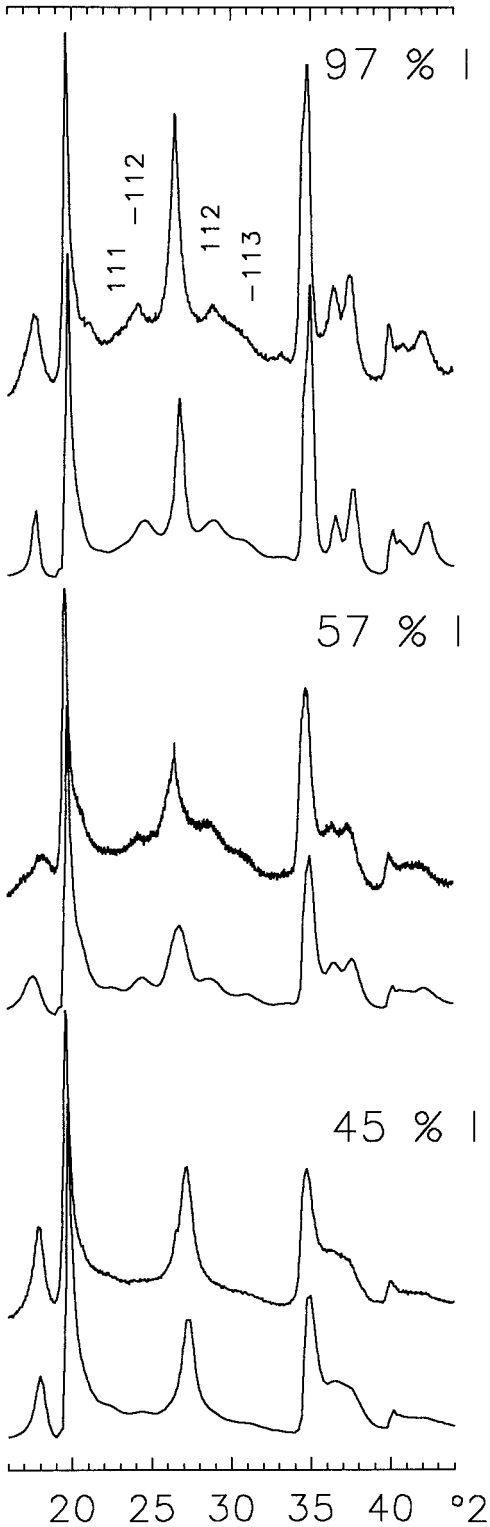

FIGURE 3. Observed (upper) and calculated (lower) XRD patterns of randomly oriented I/S for polytype analysis. The numbers above the reflections correspond to their *hkl* indexes. The parameters used in the calculations are as follows. For 45% I = Cis (%) = 70, P_0 = 0.8, P_{60} = 1. For 57% I = Cis (%) = 55, P_0 = 0.9, P_{60} = 0.5. For 97% I = Cis (%) = 45, P_0 = 0.55, P_{60} = 0.2.

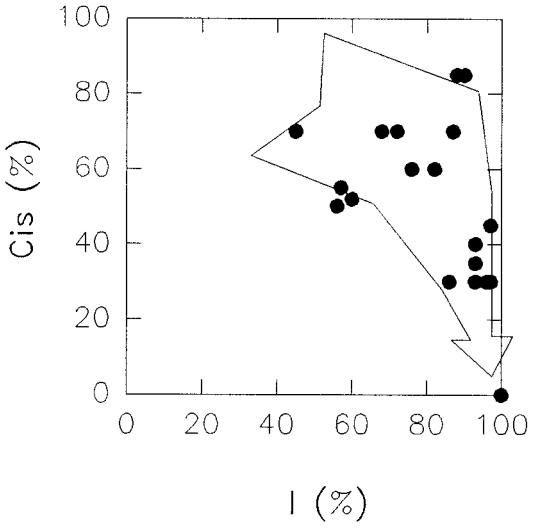

FIGURE 4. Percent cis-vacancy vs. percent illite in I/S. The arrow through the data shows the trend with progressive illitization.

taminant in sample 82-36a, which contains 1.5% P_2O_5. Although no P-bearing mineral was found in this sample, both Na and Ca seem anomalously high, considering that it contains 88% illite. We detected gypsum in sample 82-17ff by XRD, and quartz in samples 82-32o and 82-36a, but their amounts could not be quantified because of interference from I/S X-ray peaks. Hence, no correction was performed for these samples.

Most of the structural formulae listed in Table 5 seem reasonable for I/S clay minerals based on octahedral occupancies close to ideal (4.00 cations), and calculated layer charges that are typical considering the layer compositions (percent illite in I/S) of the minerals. For sample 82-36a, the layer charge seems anomalously high, probably due to an excess of Na and perhaps Ca from suspected contamination.

Both total interlayer charge and the fixed cation content ($K + NH_4$) of our I/S samples increase systematically with an increasing percent of illite (Fig. 5), although fixed cation content correlates better than layer charge. The poorer correlation between interlayer charge and the percent of illite may be due to the small amounts of Ca and Na mineral impurities, which would increase the calculated interlayer charge and cause greater scatter of the data. In the plot involving fixed cation content (Fig. 5a), the interlayer charge for the illite end-member extrapolates to 1.5, a value essentially identical to the one determined by Środoń et al. (1986) in a study of I/S from bentonite. Our results show that the bentonite I/S samples contain considerable amounts of NH_4, averaging between 9 and 22% of the total fixed cation content. Increasing illitization does not affect the octahedral charge systematically, but results in a progressive increase of the tetrahedral charge (Fig. 6). This is in agreement with what is generally found in other studies of I/S (Hower 1981; Środoń et al. 1986; Lindgreen et al. 1991).

Atomic force microscope analysis

AFM analysis indicates that our I/S samples consist of irregular, fine-grained plates that show no major morpho-

TABLE 4. Chemical composition of size-fractionated I/S in terms of weight percent oxide except for N, which is expressed in elemental weight percent

Sample	SiO_2	Al_2O_3	Fe_2O_3	TiO_2	MnO	MgO	K_2O	Na_2O	CaO	N	Total
S-2	57.0	18.0	4.3	0.1	<0.05	5.7	1.0	1.0	1.3	0.05	88.6
1-87	56.0	19.4	8.1	1.2	<0.05	1.6	0.5	0.9	1.6	0.05	89.4
2-86	58.2	17.4	9.1	1.1	<0.05	1.8	0.5	0.9	1.5	0.05	90.5
9	50.5	25.4	4.2	0.5	<0.05	2.2	6.2	0.1	1.3	0.13	90.4
11a	53.2	26.6	1.9	0.1	<0.05	2.7	5.5	0.1	1.1	0.20	91.5
11b	53.7	24.7	2.1	0.2	<0.05	2.9	4.4	0.2	1.5	0.17	90.0
14b	53.3	24.8	1.9	0.2	<0.05	3.3	5.3	0.3	1.1	0.19	90.4
82-2s	53.0	25.1	2.5	0.2	<0.05	3.2	4.1	<0.1	1.4	0.18	89.7
82-16-11b	53.8	25.3	2.0	0.5	0.05	3.0	4.9	0.5	1.1	0.19	91.2
82-17ff	48.6	24.3	5.0	1.3	<0.05	2.5	5.0	0.6	1.5	0.22	90.1
82-19g	49.9	26.0	2.8	1.9	<0.05	2.4	2.8	0.2	1.9	0.11	87.9
83-1e	52.1	25.0	2.1	0.2	<0.05	3.5	4.2	<0.1	1.2	0.16	88.6
R-80	57.2	22.3	2.7	0.1	<0.05	3.5	2.9	2.0	0.2	0.10	90.9
82-29	49.9	27.7	4.0	0.6	<0.05	2.4	6.4	<0.1	<0.1	0.38	90.9
82-32o	50.3	23.8	5.7	0.5	<0.05	2.3	7.8	0.1	<0.1	0.13	90.7
82-32u	51.4	27.2	2.8	0.6	<0.05	2.5	6.6	<0.1	<0.1	0.29	91.4
82-36a	47.6	26.6	3.1	0.1	<0.05	2.2	6.5	**0.6**	1.2	0.39	87.7
82-36b	49.2	27.1	3.3	0.2	<0.05	2.4	6.4	0.1	0.9	0.29	90.0
82-37c	53.7	23.8	1.0	0.1	<0.05	4.1	7.6	<0.1	0.3	0.13	90.8
82-38	51.3	25.2	2.7	0.2	<0.05	3.4	6.7	<0.1	0.3	0.15	90.0
NI-6	49.7	26.8	2.8	0.4	nd	3.3	8.4	0.1	0.2	0.13	91.9
WDH-25	48.9	28.9	2.2	0.2	0.05	2.3	7.8	0.1	0.2	0.17	90.9
3-1	51.9	27.5	0.8	0.2	<0.05	2.7	4.4	0.2	0.7	0.56	89.1
26-59	51.7	24.0	3.0	1.1	<0.05	3.5	5.4	0.1	1.6	0.3	90.8
26-171	51.0	26.4	1.2	1.2	<0.05	2.8	4.9	0.4	1.0	0.32	89.1
CPO-5	48.6	26.0	2.2	0.2	0.06	2.8	7.9	0.6	0.1	0.23	88.46
SWE-79	50.3	28.4	1.1	0.1	<0.05	2.5	6.4	0.2	0.6	0.31	89.1
WAL-14	50.1	28.3	1.7	0.1	0.07	2.3	8.3	0.1	0.6	0.09	91.6

Note: Mn was not determined for NI-6. Bold value is discussed in the text.

TABLE 5. Structural formulae of I/S on the basis O_{20} $(OH)_4$

Sample	Si	$^{[4]}$Al	$^{[6]}$Al	Fe	Ti	Mn	$^{[6]}$Mg	K	Na	Ca	$Mg_{int.}$	NH_4	Ch.	Σ oct.
S-2	7.72	0.28	2.58	0.45	0.01	0	1.03	0.18	0.25	0.19	0.13	0.03	1.09	4.07
1-87	7.57	0.43	2.72	0.84	0.06	0	0.33	0.09	0.24	0.24	0	0.03	0.83	3.95
2-86	7.73	0.27	2.55	0.95	0.07	0	0.36	0.08	0.24	0.22	0	0.03	0.79	3.93
9	6.93	1.07	3.09	0.44	0.01	0	0.45	1.10	0.03	0.17	0	0.08	1.54	3.99
11a	7.09	0.91	3.27	0.19	0.01	0	0.54	0.94	0.02	0.16	0	0.11	1.39	4.02
11b	7.24	0.76	3.17	0.22	0.02	0	0.58	0.75	0.05	0.22	0	0.10	1.34	4.00
14b	7.19	0.81	3.13	0.20	0.02	0	0.67	0.91	0.06	0.16	0	0.11	1.41	4.02
82-2s	7.17	0.83	3.17	0.24	0.02	0	0.64	0.71	0.01	0.20	0	0.10	1.22	4.08
82-16-11b	7.15	0.85	3.16	0.20	0.05	0.01	0.61	0.86	0.07	0.15	0	0.11	1.34	4.02
82-17ff	6.80	1.20	2.81	0.52	0.12	0	0.53	0.89	0.16	0.23	0	0.13	1.64	3.99
82-19g	7.03	0.97	3.34	0.29	0	0.01	0.51	0.50	0.04	0.28	0	0.07	1.18	4.11
83-1e	7.14	0.86	3.17	0.22	0.02	0	0.71	0.74	0.01	0.18	0	0.09	1.21	4.12
R-80	7.57	0.43	3.05	0.27	0.01	0	0.68	0.48	0.51	0.02	0	0.06	1.09	4.01
82-29	6.77	1.23	3.21	0.40	0.01	0	0.48	1.10	0.01	0.01	0	0.22	1.34	4.12
82-32o	6.97	1.03	2.86	0.60	0.06	0	0.47	1.37	0.03	0.01	0	0.08	1.50	3.98
82-32u	6.91	1.09	3.22	0.28	0.06	0	0.50	1.13	0.01	0.01	0	0.17	1.33	4.06
82-36a	6.71	1.29	3.13	0.33	0.01	0	0.46	1.16	**0.17**	0.18	0	0.24	**1.93**	3.94
82-36b	6.78	1.22	3.18	0.35	0.02	0	0.48	1.13	0.02	0.13	0	0.17	1.59	4.03
82-37c	7.29	0.71	3.10	0.08	0.01	0	0.82	1.31	0.01	0.04	0	0.08	1.46	4.02
82-38	7.04	0.96	3.12	0.26	0.02	0	0.68	1.17	0.01	0.05	0	0.09	1.36	4.09
NI-6	6.77	1.23	3.08	0.28	0.04	0	0.67	1.47	0.04	0.03	0	0.08	1.63	4.07
WDH-25	6.68	1.32	3.34	0.23	0.02	0.01	0.47	1.37	0.03	0.02	0	0.10	1.54	4.08
3-1	6.99	1.01	3.41	0.08	0.02	0	0.55	0.77	0.06	0.10	0	0.33	1.37	4.06
26-59	7.13	0.87	3.02	0.31	0.01	0	0.73	0.96	0.04	0.10	0	0.18	1.38	4.07
26-171	7.00	1.00	3.30	0.13	0.03	0	0.59	0.86	0.09	0.13	0	0.19	1.41	4.05
CPO-5	6.84	1.16	3.15	0.23	0.02	0.01	0.58	1.42	0.15	0.01	0	0.14	1.73	4.00
SWE-79	6.85	1.15	3.40	0.11	0.01	0	0.52	1.11	0.05	0.09	0	0.18	1.52	4.05
WAL-14	6.80	1.20	3.33	0.17	0.01	0.01	0.47	1.44	0.02	0.08	0	0.05	1.67	4.00

Note: Ch. stands for interlayer charge. Bold values are discussed in the text.

logical changes through the entire range of I/S composition (Fig. 7). In many cases, we found aggregates of particles probably due to the fact that we did not use a dispersant during sample preparation. For our size analysis, we only measured the dimensions of completely separated particles. The I/S clay particles were nearly always flake-shaped, with rounded edges. Elongate particles with irregular shapes were observed in a few cases. However, no relationship exists between the presence of elongate particles and the degree of illitization. Only two samples (S-2 and R-80) had a somewhat different morphology, containing very flat particles with relatively straight edges. I/S in the S-2 sample is hydrothermal in origin rather than diagenetic, which might explain its different morphology. Nevertheless, R-80 has a diagenetic origin and a possible explanation for its more regularly shaped particles may be that the I/S has a kaolinite precursor rather than a smectite precursor. R-80 is from a Carboniferous bentonite located in a section with abundant coal seams, which are commonly associated with tonsteins (volcanic ash layers altered to kaolinite). Also, the particles in samples R-80 and S-2 were more completely dispersed (Fig. 7c). The reason for the exceptional dispersion of particles in R-80 is that Na is the dominant interlayer cation in this sample.

Particle dimension measurements support our finding that no major changes except for thickening occur in particle morphology with degree of illitization. This result is best displayed by the parameters mean diameter, aspect ratio, and thickness of the particles. Mean diameter is defined as the square root of the product of the length and width (as defined in the methods section) of each particle ($\sqrt{l \cdot w}$). Aspect ratio is defined as the ratio l/w.

Frequency diagrams (Fig. 8) for several representative samples show no major changes in the diameter and aspect ratio of the particles with increasing illite content. In contrast, average particle diameters of hydrothermal I/S do show very large changes as illite content increases. Altaner and Ylagan (1997) summarized data from different studies of hydrothermal I/S, in which particle diameter increased from ~80 to ~2000 nm for an illite content of 40 to 100%. In our study, particle thickness changes in a manner similar to that observed in other morphological studies of I/S (Eberl et al. 1990; Lindgreen et al. 1992; Inoue and Kitagawa et al. 1994): As illite content increases, the distribution flattens and the average and maximum thicknesses increase.

Particle diameter, aspect ratio, and thickness are plotted vs. percent illite for all samples in Figure 9.'Mean'' refers to the average value. ''Maximum'' refers to the maximum observed value after eliminating 10% of the data with the highest values. In this way we avoided anomalously large measurements. Neither diameter nor aspect ratio change in a significant way with degree of illitization. In addition, particle diameter showed no correlation with particle thickness (not shown).

From 0 to ~50% illite, the average thickness of I/S particles remains relatively constant at ~2 nm, and progressively increases to ~10 nm for 100% illite (Fig. 9c). Figure 8 shows that, for smectitic I/S, half of the particles are 1 nm thick and the rest are distributed among greater thicknesses. The presence of particles thicker than 1 nm

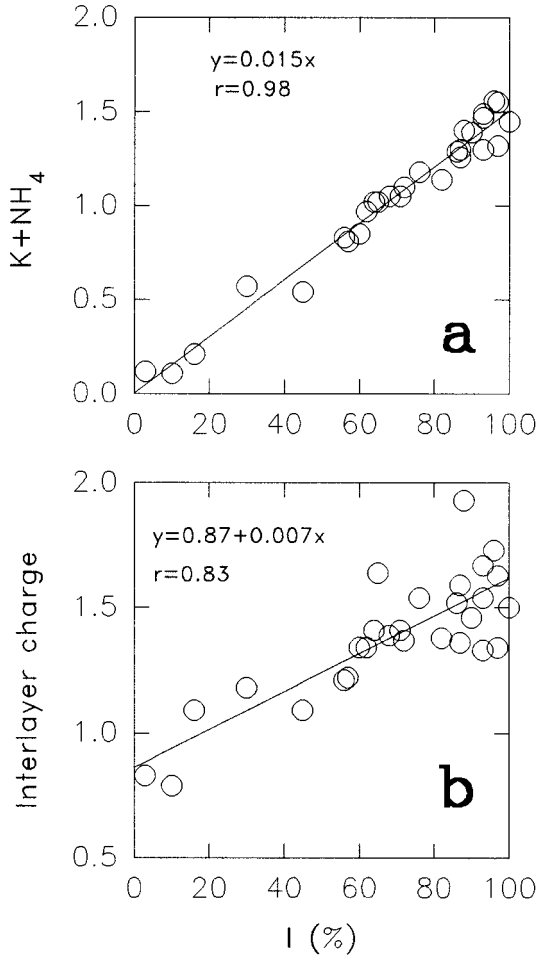

FIGURE 5. $K + NH_4$ content vs. percent illite in I/S (**a**) and interlayer charge vs. percent illite in I/S (**b**).

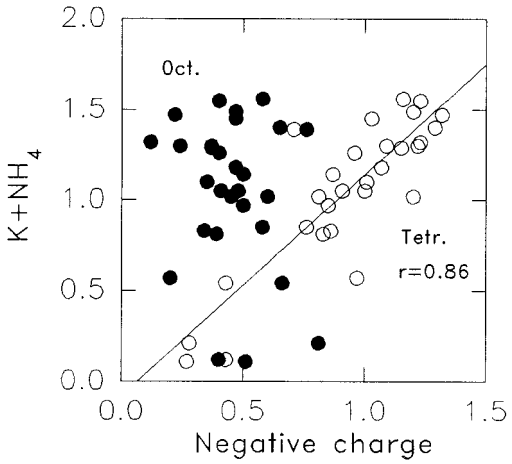

FIGURE 6. $K + NH_4$ content vs. I/S octahedral (●) and tetrahedral charge (○). Charge develops in the tetrahedral sheet during illitization.

may be due to incomplete dispersion because we did not Li- or Na-exchange our samples before AFM analysis. On the other hand, AFM analysis is carried out under normal pressure and humidity conditions. In such conditions, smectite particles should be hydrated and have thicknesses of 1.2–1.5 nm.

Oxygen isotope analysis

Our oxygen isotope data present various trends depending on the amount of illite in I/S (Table 6, Fig. 10). For smectitic I/S, we do not have enough samples to describe any trend. The sample with a $\delta^{18}O$ value of 23‰ is from Almería (Spain). Previous oxygen and hydrogen isotope studies of the bentonite and quartz veins contained in it (Delgado 1994) are consistent with an initial incomplete alteration of the tuff by hydrothermal fluids (~80 °C) followed by a pervasive alteration by meteoric waters (~20 °C) having a composition of −5‰.

Cretaceous samples (solid dots), which are from the same general area, show little variation in their O isotope composition despite having a relatively large range of illite content (30–80% illite). In each one of the three series of more illitic samples (open symbols: circles, squares, and inverted triangles), I/S samples do show an isotope composition variation, becoming depleted in ^{18}O with increasing illite, although one of the Devonian bentonites (inverted open triangles) has a much lower $\delta^{18}O$ value than the other Devonian bentonite I/S samples. Devonian samples are from two different locations (Tables 1 and 6). Sample 82-36b, the one plotting below the other Devonian samples, is from the same location as 82-37c and 82-38, hence there is no evident reason for its lower $\delta^{18}O$ value. Three of the four Ordovician samples analyzed (open circles) are from the same location and one is from a different locality. This last one (SWE-79) has the lowest $\delta^{18}O$ value, but it plots consistently with the others.

DISCUSSION

The absence of major morphological changes (in particle shape or size) in the bentonite I/S samples investigated by us provides the best indication that smectite was transformed into illite by means of an SST mechanism. Reactions involving dissolution of the smectite precursor and precipitation of the I/S (or illite) product likely would have been accompanied by morphological changes reflecting the different conditions in which the new material was precipitating, as has been commonly observed for hydrothermal I/S (Inoue 1986; Yau et al. 1987; Inoue et al. 1988; Inoue and Kitagawa 1994). Although particle thickening occurs during smectite illitization, we interpret this change to represent coalescence of smectite sites as interlayers (c* unit cells from one octahedral sheet to the adjacent octahedral sheet) become illitic and interlayer K is fixed. The fact that our study includes I/S samples from different locations rather than from a single locality, supports the idea that the SST mechanism controls illitization in bentonite lithologies in general. Morphological features

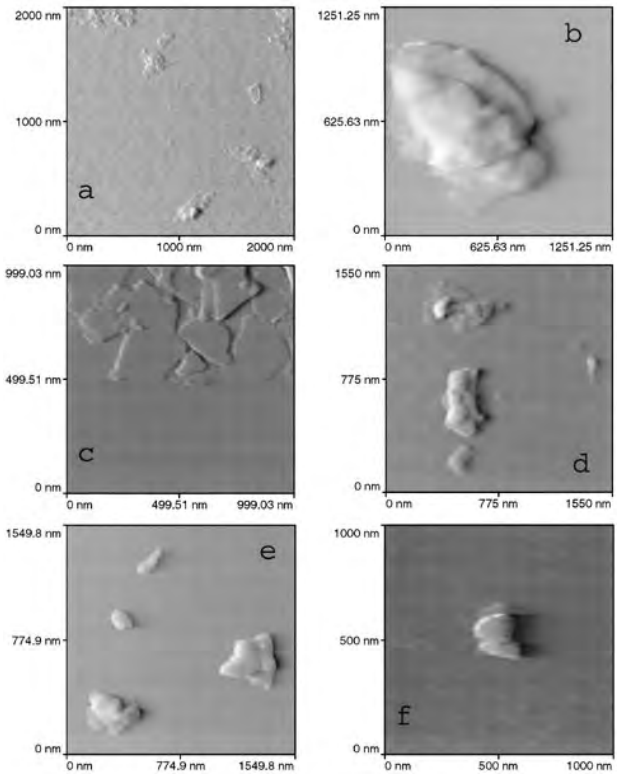

FIGURE 7. AFM images of some selected I/S samples. (**a**) 1-87 = 3% illite, (**b**) 82-19g = 30% illite, (**c**) R-80 = 45% illite, (**d**) 82-2s = 57% illite, (**e**) 82-36b = 87% illite, and (**f**) 82-32o = 100% illite. Dimension measurements were performed only on completely separated, flat-topped particles. Corrugations on particle surfaces correspond to aggregates rather than growth steps on single particles.

of all I/S samples behave the same way as illitization proceeds, irrespective of their location.

Other analytical results from our bentonite I/S series are not as conclusive as AFM data to the interpretation of reaction mechanism, although they also point toward an SST mechanism or can be considered consistent with it. The interlayer ordering parameter (R) progressively increases with percent illite, even showing non-integral values (Table 3). The progressive and gradual changes in R are more consistent with an SST mechanism than with a DP mechanism because the latter is more likely to have generated distinct integral R values, which depends on the environmental conditions, causing greater discontinuities in the ordering succession. Also, the lack of a trend from a more disordered $1M_d$ to a more ordered $1M$ illite with progressive illitization (Table 3) indicates some inheritance of the stacking disorder from the original smectite. A DP mechanism would have developed a clearer transition toward the $1M$ polytype (Eberl et al. 1987; Inoue and Kitagawa 1994). McCarty and Reynolds (1995) also found no correlation between 3-dimensional ordering and percent illite for bentonite containing from 9 to 33% expandable layers. Fixed cation content also increases continuously with percent illite throughout the I/S series (Fig. 5), suggesting a single reaction mechanism.

Our data are in contrast with results of Środoń et al. (1986), who concluded that the variation of fixed K with percent illite should be represented by two straight lines, one for R = 0 I/S and the other for R > 0. They interpreted their results in terms of a transformation mechanism in which illitization of smectite sites in I/S with R > 0 needs a higher charge development than for smectite sites in I/S with R = 0. We found that a single straight line fits our data regardless of whether or not the results for I/S with R = 0 are included. A possible explanation for the different results is that our fixed cation data include both NH_4 and K whereas the Środoń et al. (1986) study includes only K. In a later study, Środoń et al. (1992) concluded that the variation between fixed cation content and percent illite, as measured by TEM determinations of particle thickness, was best represented by a single straight line. They considered the TEM measurements of percent illite to be more accurate than the corresponding XRD measurements, because XRD underestimates the proportion of smectite in very illitic I/S clays. Altaner et al. (1988) also found that XRD underestimates the proportion of smectite compared to nuclear magnetic resonance (NMR) for very illitic I/S samples. Our AFM data of particle thickness are inappropriate to use as mea-

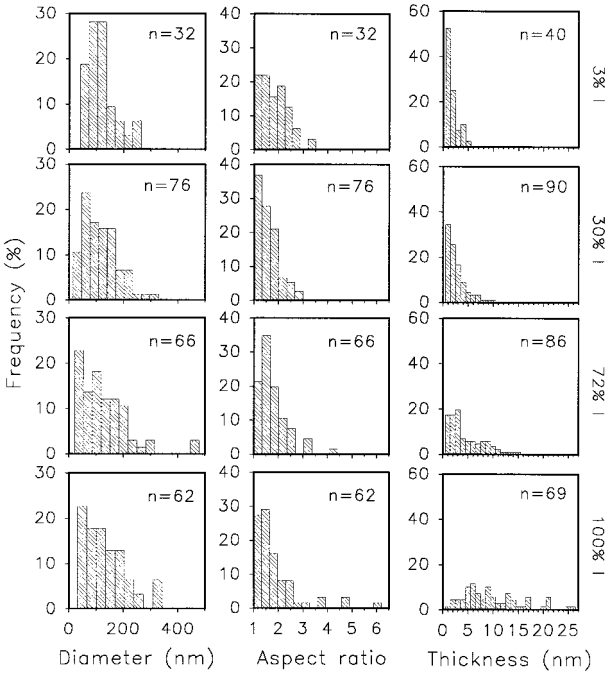

FIGURE 8. Frequency diagrams of calculated particle diameter ($\sqrt{l \cdot w}$), aspect ratio (l/w), and thickness for four samples. Each row corresponds to the same sample. Percent illite in I/S is indicated at the right of each row. "n" is the number of analyzed particles.

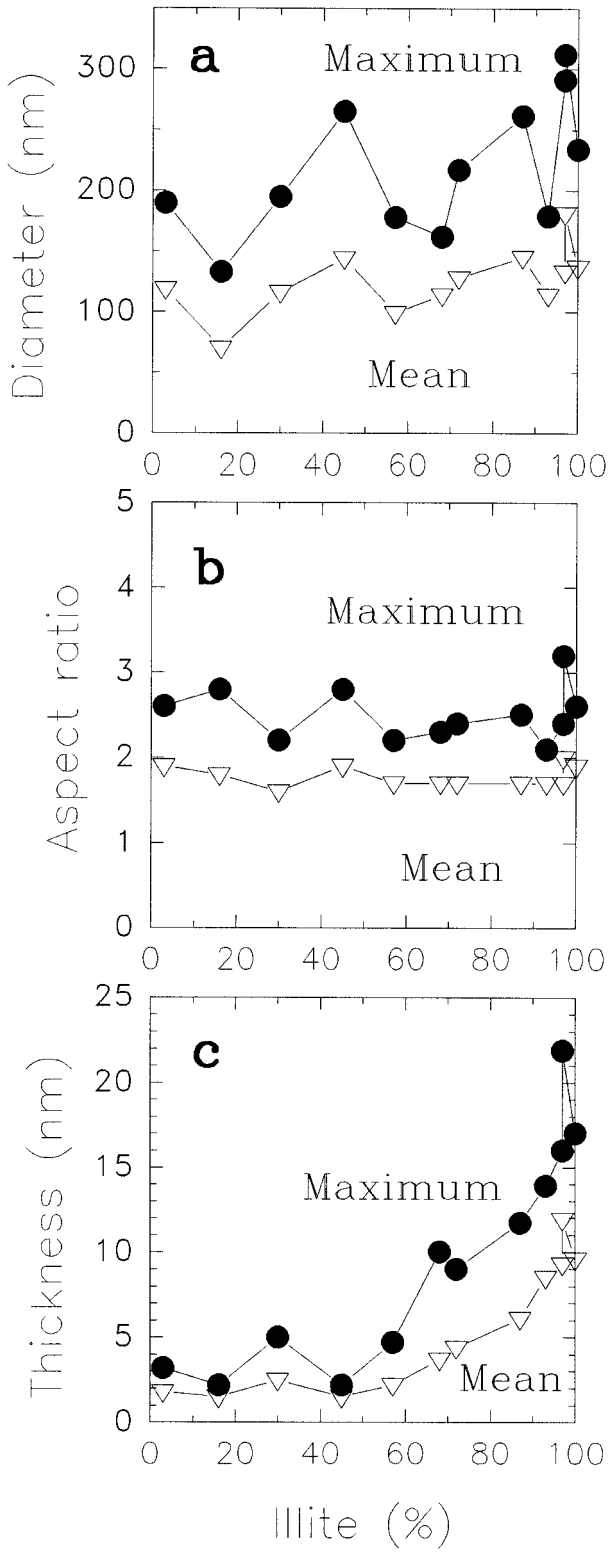

FIGURE 9. (**a**) Calculated diameter of particles ($\sqrt{l \cdot w}$) vs. percent illite in I/S; (**b**) particle aspect ratio (l/w) vs. percent illite; (**c**) particle thickness vs. percent illite. Mean refers to average of all values. Maximum refers to the highest value, excluding the upper 10%. Only thickness shows a significant change with illitization.

TABLE 6. Oxygen isotope composition (in ‰ $\delta^{18}O$) of the I/S samples

Sample	$\delta^{18}O$	Sample	$\delta^{18}O$
S-2	23.0	82-29	16.6
1-87	9.8	82-32o	15.6
2-86	11.5	82-32u	16.8
9	13.0	82-36b	12.6
11a	11.8	82-37c	18.1
11b	13.4	82-38	17.0
14b	12.6	NI-6	13.2
82-2s	12.3	WDH-25	13.8
82-16-11b	12.8	3-1	17.3
82-17ff	12.8	26-59	15.9
82-19g	13.5	26-171	18.8
83-1e	12.7	SWE-79	13.1
R-80	16.4		

sures of percent illite because of incomplete dispersal of particles, as discussed above.

Progressive changes in the 2:1 layer include a greater negative charge (produced mainly by tetrahedral Al for Si substitution) and conversion from cis-vacant I/S to trans-vacant I/S (Fig. 4). The observed chemical and structural changes indicate that significant lattice rearrangement occurs during smectite illitization even with an SST mechanism. However, these structural changes are much less systematic and less extensive than those observed for hydrothermal I/S, where a DP mechanism is clearly indicated [compare the XRD polytype patterns in Fig. 5 of Inoue et al. (1987) with our polytype patterns in Fig. 3, and cis/trans occupancy variation with illite in Fig. 5 of Drits et al. (1996) with the same variation in Fig. 4 of this study], which also supports an SST mechanism for illitization in bentonite. We interpret the broad correlation between percent illite and cis/trans occupancy in our samples (Fig. 4) to be due to the fact that structural changes are somewhat hindered by an SST mechanism. Also, because our samples are from different loca-

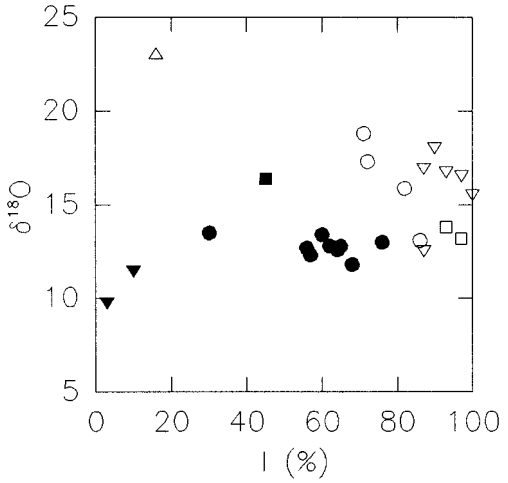

FIGURE 10. Oxygen isotope composition vs. percent illite of the I/S clays. ▼ = Miocene, ● = Cretaceous, ■ = Carboniferous, △ = Pliocene, ▽ = Devonian, ○ = Ordovician, □ = Silurian.

tions, the cis/trans occupancy of the original smectites could be different, thereby affecting their path lines in Figure 4. We propose that illitization follows an SST mechanism in which there is simultaneous rearrangement of a significant fraction of atoms within the individual or adjacent 2:1 layers. This local rearrangement allows for structural changes and chemical substitutions within the area where it occurs.

Oxygen isotope results in our study are difficult to interpret with respect to illitization mechanism because the samples are from many different locations and must have experienced very different conditions of formation and diagenesis. Previous studies have shown that $\delta^{18}O$ values of bentonite I/S generally decrease with increasing percent illite, although there is typically a wide range in $\delta^{18}O$ for a given illite content (Yeh and Savin 1977; Eslinger and Yeh 1986). In our study, the Cretaceous I/S samples from Montana are from the same area (filled circles in Fig. 10), but do not show any appreciable variation in $\delta^{18}O$ over the range of 30–80% illite. Although lack of isotopic variation could be interpreted as precluding any major clay dissolution, this conclusion seems difficult to justify in light of the more systematic isotopic variations found in the study of Eslinger and Yeh (1986).

In summary, the mechanism of illitization in bentonites seems to be a solid-state reaction that allows for rearrangement of atoms at local scale producing structural (cis-trans occupancy) and chemical changes in the 2:1 layer. This is supported by different facts: the lack of I/S particle morphology alteration during illitization, except for the fact that K fixation causes interlayers to coalesce, which results in thicker particles; the progressive and gradual change of ordering R values; the lack of a trend from a less ordered $1M_d$ to a more ordered 1*M* illite polytype; and the fact that the transition from a cis- to a trans-vacant structure during illitization is somewhat hindered as compared to the transformation that operates in hydrothermal systems, in which a DP mechanism seems to occur.

Acknowledgments

We thank Warren Huff for providing some of the samples studied, Emilio Reyes and Rafael Núñez for the oxygen isotope analysis and help for its interpretation, and Robert C. Reynolds for discussion of some of the XRD results. We also thank Holger Lindgreen and an anonymous reviewer for their thoughtful comments, which helped to improve this paper. This study was financed by the Petroleum Research Fund, grant 27767-AC.

References cited

Ahn, J. and Peacor, D. (1986) Transmission electron microscope data for rectorite: implication for the origin and structure of ''fundamental particles.'' Clays and Clay Minerals, 34, 180–186.

Altaner, S. (1985) Potassium metasomatism and diffusion in Cretaceous K-bentonites from the disturbed belt, north-western Montana and in the Middle Devonian Tioga K-bentonite, eastern USA, 193 p. Ph.D. thesis, University of Illinois, Urbana.

Altaner, S. and Grim, R. (1990) Mineralogy, chemistry, and diagenesis of tuffs in the Sucker Creek Formation (Miocene), Eastern Oregon. Clays and Clay Minerals, 38, 561–572.

Altaner, S. and Ylagan, R. (1997) Comparison of structural models of mixed-layer illite-smectite and reaction mechanisms of smectite illitization. Clays and Clay Minerals, 45, 517–533.

Altaner, S., Hower, J., Whitney, G., and Aronson, J. (1984) Model for K-bentonite formation: Evidence from zoned K-bentonites in the disturbed belt, Montana. Geology, 12, 412–415.

Altaner, S., Weiss, C. Jr., and Kirkpatrick, J. (1988) Evidence from ^{29}Si NMR for the structure of mixed-layer illite-smectite clay minerals. Nature, 331, 699–702.

Amouric, M. and Olives, J. (1991) Illitization of smectite as seen by high-resolution transmission electron microscopy. European Journal of Mineralogy, 3, 831–835.

Awwiller, D. (1993) Illite-smectite formation and potassium mass transfer during burial diagenesis of mudrocks: A study from the Texas Gulf coast Paleocene-Eocene. Journal of Sedimentary Petrology, 63, 501–512.

Bayliss, P. (1986) Quantitative analysis of sedimentary minerals by powder X-ray diffraction. Powder Diffraction, 1, 37–39.

Bell, T. (1986) Microstructure in mixed-layer illite-smectite and its relationship to the reaction of smectite to illite. Clays and Clay Minerals, 34, 146–154.

Bergstrom, S. and Nilsson, R. (1974). Age and correlation of the Middle Ordovician bentonites on Bornholm. Bulletin of the Geological Society of Denmark, 23, 27–48.

Bethke, C., Vergo, N., and Altaner, S. (1986) Pathways of smectite illitization. Clays and Clay Minerals, 34, 125–135.

Borthwick, J. and Harmon, R. (1982) A note regarding ClF_3 as an alternative to BrF_5 for oxygen isotope analysis. Geochimica et Cosmochimica Acta, 46, 1665–1668.

Brun, J. and Chagnon, A. (1979) Rock stratigraphy and clay mineralogy of volcanic ash beds from the Black River and Trenton Groups (Middle Ordovician) of southern Quebec. Canadian Journal of Earth Sciences, 16, 1499–1507.

Buatier, M., Peacor, D., and O'Neil, J. (1992) Smectite-illite transition in Barbados accretionary wedge sediments: TEM and AEM evidence for dissolution/crystallization at low temperature. Clays and Clay Minerals, 40, 65–80.

Cameron, T. and Anderson, T. (1980) Silurian metabentonites in County Down, Northern Ireland. Geological Journal, 15, 59–75.

Cetin, K. and Huff, W. (1995) Layer charge of the expandable component of illite-smectite in K-bentonite as determined by alkylammonium ion exchange. Clays and Clay Minerals, 43, 150–158.

Cuadros, J. and Linares, J. (1996) Experimental kinetic study of the smectite-to-illite transformation. Geochimica et Cosmochimica Acta, 60, 439–453.

Cuadros, J. and Altaner, S. (1998) Compositional and structural features of the octahedral sheet in mixed-layer illite-smectite from bentonites. European Journal of Mineralogy, 10, 111–124.

Culmo, R. (1969) Automatic microdetermination of carbon, hydrogen, and nitrogen: Improved combustion train and handling techniques. Mikrochimica Acta, 1, 175–180.

Delgado, A. (1994) Isotopic study of the diagenetic and hydrothermal processes related to bentonite genesis (Cabo de Gata, Almería). Ph.D. thesis, Universidad de Granada, Granada, Spain (in Spanish).

Drits, V., Salyn, A., and Šucha, V. (1996) Structural transformations of interstratified illite-smectites from Dolná Ves hydrothermal deposits: dynamics and mechanisms. Clays and Clay Minerals, 44, 181–190.

Dunoyer de Segonzac, G. (1970) The transformation of clay minerals during diagenesis and low-grade metamorphism: A review. Sedimentology, 15, 281–346.

Eberl, D. (1978) The reaction of montmorillonite to mixed-layer clay: the effect of interlayer alkali and alkaline earth cations. Geochimica et Cosmochimica Acta, 42, 1–7.

Eberl, D. (1993) Three zones for illite formation during burial diagenesis and metamorphism. Clays and Clay Minerals, 41, 26–37.

Eberl, D. and Środoń, J. (1988) Ostwald ripening and interparticle-diffraction effects for illite crystals. American Mineralogist, 73, 1335–1345.

Eberl, D., Środoń, J., Lee, M., Nadeau, P., and Northrop, H. (1987) Sericite from the Silverton caldera, Colorado: Correlation among structure, composition, origin, and particle thickness. American Mineralogist, 72, 914–934.

Eberl, D., Środoń, J., Kralik, M., Taylor, B., and Peterman, Z. (1990)

Ostwald ripening of clays and metamorphic minerals. Science, 248, 474–477.

Elliott, W., Aronson, J., Matisoff, G., and Gautier, D. (1991) Kinetics of the smectite to illite transformation in the Denver basin: Clay mineral, K-Ar data, and mathematical model results. American Association of Petroleum Geologists Bulletin, 75, 436–462.

Eslinger, E. and Yeh, H. (1986) Oxygen and hydrogen isotope geochemistry of Cretaceous bentonites and shales from the Disturbed Belt, Montana. Geochimica et Cosmochimica Acta, 50, 59–68.

Güven, N. (1988) Smectites. In Mineralogical Society of America Reviews in Mineralogy, 19, 497–560.

Harvey, C. and Browne, P. (1991) Mixed-layer clay geothermometry in the Wairakei geothermal field, New Zealand. Clays and Clay Minerals, 39, 614–621.

Hower, J. (1981) Shale diagenesis. In F.J. Longstaffe, Ed., Clays and the resource geologist, p. 40–60. Mineralogical Association of Canada, Calgary.

Hower, J., Eslinger, E., Hower, M., and Perry, E. (1976) Mechanism of burial metamorphism of argillaceous sediments: I. Mineralogical and chemical evidence. Geological Society of America Bulletin, 87, 725–737.

Huang, W., Longo, J., and Pevear, D. (1993) An experimentally derived kinetic model for smectite-to-illite conversion and its use as a geothermometer. Clays and Clay Minerals, 41, 162–177.

Inoue, A. (1986) Morphological change in a continuous smectite-to-illite conversion series by scanning and transmission electron microscopies. Journal of the College of Arts and Sciences, Chiba University, B-19, 23–33.

Inoue, A. and Kitagawa, R. (1994) Morphological characteristics of illitic clay minerals from a hydrothermal system. American Mineralogist, 79, 700–711.

Inoue, A., Kohyama, N., Kitagawa, R., and Watanabe, T. (1987) Chemical and morphological evidence for the conversion of smectite to illite. Clays and Clay Minerals, 35, 111–120.

Inoue, A., Velde, B., Meunier, A., and Touchard, G. (1988) Mechanism of illite formation during smectite-to-illite conversion in a hydrothermal system. American Mineralogist, 73, 1325–1334.

Inoue, A., Watanabe, T., Kohyama, N., and Brusewitz, A. (1990) Characterization of illitization of smectite in bentonite beds at Kinnekulle, Sweden. Clays and Clay Minerals, 38, 241–249.

Keller, W., Reynolds, R., and Inoue, A. (1986) Morphology of clay minerals in the smectite-to-illite conversion series by scanning electron microscopy. Clays and Clay Minerals, 34, 187–197.

Kitagawa, R., Inoue, A., and Kohyama, N. (1994) Surface microtopography of interstratified mica and smectite from the Goto pyrophyllite deposit, Japan. Clay Minerals, 29, 709–715.

Lanson, B. and Champion, D. (1991) The I/S-to-illite reaction in the late stage diagenesis. American Journal of Science, 291, 473–506.

Lindgreen, H. and Hansen, P. (1991) Ordering of illite-smectite in Upper Jurassic claystones from the North Sea. Clay Minerals, 26, 105–125.

Lindgreen, H., Jacobsen, H., and Jakobsen, H. (1991) Diagenetic structural transformations in North Sea Jurassic illite-smectite. Clays and Clay Minerals, 39, 54–69.

Lindgreen, H., Garnaes, J., Besenbacher, F., Laegsgaard, E., and Stensgaard, I. (1992) Illite-smectite from the North Sea investigated by scanning tunneling microscopy. Clay Minerals, 27, 331–342.

McCarty, D. and Reynolds, R. (1995) Rotationally disordered illite-smectite in paleozoic K-bentonites. Clays and Clay Minerals, 43, 271–284.

Moore, D. and Reynolds, R. (1989) Identification of mixed-layer clay minerals. In X-ray diffraction and the identification and analysis of clay minerals, p. 241–271. Oxford University Press, New York.

Nadeau, P., Wilson, M., McHardy, W., and Tait, J. (1985) The conversion of smectite to illite during diagenesis: evidence from some illitic clays from bentonites and sandstones. Mineralogical Magazine, 49, 393–400.

Pollastro, R. (1985) Mineralogical and morphological evidence for the formation of illite at the expense of illite-smectite. Clays and Clay Minerals, 33, 265–274.

Reynolds, R. (1993) Three-dimensional X-ray powder diffraction from disordered illite: simulation and interpretation of the diffraction patterns. In CMS Workshop Lectures, 5, 44–78.

Roberson, H. and Lahann, R. (1981) Smectite to illite conversion rates: Effects of solution chemistry. Clays and Clay Minerals, 29, 129–135.

Robert, M., Elsass, F., Andreoli, C., and Środoń, J. (1991) The cycle of 2:1 clay minerals transformation in sediments and soils. New applications of high resolution transmission microscopy. Proceedings of the 7th Euroclay Conference, Dresden, 875–879.

Shutov, V., Drits, V., and Sakharov, B. (1969) On the mechanism of a postsedimentary transformation of montmorillonite into hydromica. Proceedings of the International Clay Conference, Tokyo. Israel University Press, 523–531.

Smallwood, S. (1986) Sedimentation across the Tywi Lineament, Mid Wales. Philosophical transactions. Royal Society of London, A317, 279–288.

Środoń, J., Morgan, D., Eslinger, E., Eberl, D., and Karlinger, M. (1986) Chemistry of illite-smectite and end-member illite. Clays and Clay Minerals, 34, 368–378.

Środoń, J., Elsass, F., McHardy, W., and Morgan, D. (1992) Chemistry of illite-smectite inferred from TEM measurements of fundamental particles. Clay Minerals, 27, 137–158.

Šucha, V., Kraus, I., Gerthofferová, H., Petes, J., and Sereková, M. (1993) Smectite to illite conversion in bentonites and shales of the East Slovak basin. Clay Minerals, 28, 243–253.

Velde, B. (1984) Electron microprobe analysis of clay minerals. Clay Minerals, 19, 243–247.

Venneman, T. and Smith, H. (1990) The rate and temperature of reaction of ClF_3 with silicate minerals, and their relevance to oxygen isotope analysis. Chemical Geology, 86, 83–88.

Whitney, G. (1990) Role of water in the smectite-to-illite reaction. Clays and Clay Minerals, 38, 343–350.

——— (1992) Dioctahedral smectite reactions at elevated temperatures: Effects of K-availability, Na/K ratio and ionic strength. Applied Clay Science, 7, 97–112.

Whitney, G. and Northrop, H. (1988) Experimental investigation of the smectite to illite reaction: Dual reaction mechanism and oxygen-isotope systematics. American Mineralogist, 73, 77–90.

Yau, Y., Peacor, D., and McDowell, S. (1987) Smectite-to-illite reactions in Salton Sea shales: A transmission and analytical electron microscopy study. Journal of Sedimentary Petrology, 57, 335–342.

Yeh, H. and Savin, S. (1977) Mechanism of burial metamorphism of argillaceous sediments. 3. O-isotope evidence. Geological Society of America Bulletin, 88, 1321–1330.

Ylagan, R. (1996) Mineralogy and geochemistry associated with hydrothermal alteration of a rhyolitic hyaloclastite from Ponza Island, Italy, 153 p. Ph.D. dissertation, University of Illinois, Urbana.

Manuscript received March 18, 1997
Manuscript accepted March 9, 1998
Paper handled by Kathryn L. Nagy